

## Kelvin wave signatures in stratospheric trace constituents

Philip W. Mote and Timothy J. Dunkerton

Northwest Research Associates, Bellevue, Washington, USA

Received 31 December 2002; revised 29 October 2003; accepted 13 November 2003; published 3 February 2004.

[1] Connections, sometimes tenuous, have previously been noted between stratospheric Kelvin waves and several stratospheric trace constituents. The present study finds evidence of Kelvin wave signatures in ozone from the Microwave Limb Sounder (MLS) and Cryogenic Limb Array Etalon Spectrometer (CLAES) instruments aboard the Upper Atmosphere Research Satellite. Predominant variations near 10 days are associated with a Kelvin wave mode previously identified in MLS temperature. Variations in CLAES nitrous oxide also show some evidence of influence by this Kelvin mode. The results presented here show that the observing characteristics of the instrument can influence the derived structure and properties of Kelvin waves. *INDEX TERMS:* 0340 Atmospheric Composition and Structure: Middle atmosphere—composition and chemistry; 0341 Atmospheric Composition and Structure: Middle atmosphere—constituent transport and chemistry (3334); 3334 Meteorology and Atmospheric Dynamics: Middle atmosphere dynamics (0341, 0342); *KEYWORDS:* Kelvin wave, tropical dynamics, trace constituents

**Citation:** Mote, P. W., and T. J. Dunkerton (2004), Kelvin wave signatures in stratospheric trace constituents, *J. Geophys. Res.*, 109, D03101, doi:10.1029/2002JD003370.

### 1. Introduction

[2] On timescales less than 90 days, the dominant features in the tropical stratosphere are produced by atmospheric Kelvin waves [e.g., Wallace and Gousky, 1968]. Kelvin waves, which are equatorially trapped, perturb the temperature, wind, and trace constituent fields; they also influence stratosphere-troposphere exchange [Fujiwara *et al.*, 1998, 2001]. Observations from space-based instruments have shown the structure of Kelvin waves in temperature and have helped illuminate their influence on trace constituents. Randel [1990] examined data from the Limb Infrared Monitor of the Stratosphere (LIMS) for water vapor ( $\text{H}_2\text{O}$ ), ozone ( $\text{O}_3$ ), nitric acid ( $\text{HNO}_3$ ), and nitrogen dioxide ( $\text{NO}_2$ ). Randel found reasonable relationships between temperature perturbations and perturbations in  $\text{O}_3$  and  $\text{HNO}_3$ , but very small and retrieval-dependent perturbations in  $\text{H}_2\text{O}$  and  $\text{NO}_2$ , with  $\text{H}_2\text{O}$ 's weak signal confined to the lower stratosphere. Kawamoto *et al.* [1997] also examined LIMS data for  $\text{O}_3$  and  $\text{H}_2\text{O}$ , and, like Randel, found a weak signal of  $\text{H}_2\text{O}$  perturbations in the lower stratosphere. Shiotani *et al.* [1997] looked for Kelvin wave signatures in  $\text{H}_2\text{O}$  and  $\text{O}_3$  observations from the Cryogenic Limb Array Etalon Spectrometer (CLAES), aboard the Upper Atmosphere Research Satellite (UARS), but reported that they “could not find significant signals” in these fields. Canziani *et al.* [1994, 1995] and Canziani and Holton [1998] described variations in MLS temperature and ozone, showing that the relationship between the two fields was generally as expected from theoretical and modeling stud-

ies. Using data taken by the CRISTA instrument flying during two NASA Space Shuttle missions, each lasting just over a week, Smith *et al.* [2002] found Kelvin wave-like features in  $\text{O}_3$ , CFC-11,  $\text{HNO}_3$ ,  $\text{N}_2\text{O}$ , and  $\text{CH}_4$  that were correlated with temperature perturbations.

[3] Mote *et al.* [2002] (hereinafter M02), described Kelvin wave variations in MLS temperature data. This study extends their work by describing the variations in several trace constituents from the MLS and CLAES instruments. We examine temperature and ozone data from both MLS and CLAES, and methane, nitrous oxide, and chlorofluorocarbon (CFC)-12 from CLAES. While many other trace constituents are available on UARS, these trace constituents were chosen because their vertical profiles (a crucial determinant of Kelvin wave signatures) are quite different. Methane has almost no gradient in the lower stratosphere, but decreases sharply in the upper stratosphere; nitrous oxide and CFC-12 decrease steadily from the lower stratosphere to values near zero in the upper stratosphere; the gradient of ozone changes sign in the middle stratosphere; and water vapor has a seasonally varying vertical profile in the lower stratosphere, with two or even three changes in sign of its vertical gradient. Of these constituents, ozone has the most robust signature; nitrous oxide will also be presented; and water vapor will be presented elsewhere because its complicated vertical structure makes interpretation more difficult.

### 2. Data

[4] The Upper Atmosphere Research Satellite (UARS) [Reber *et al.*, 1993] was launched in September 1991 and collected data for ten years until science observations ceased. UARS is in an orbit inclined  $57^\circ$  to the equator at an altitude

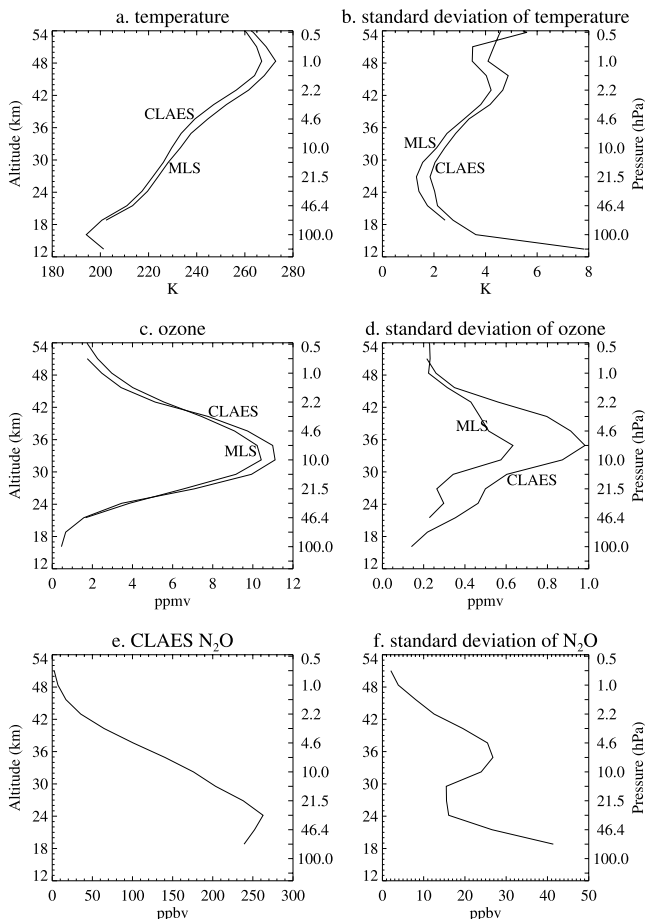


**Figure 1.** Mean profiles (left column) and standard deviations (right column) of temperature and trace constituents, as indicated, in the tropics ( $10^{\circ}\text{S}$ – $10^{\circ}\text{N}$ ).

of 585 km. Owing to orbit precession, approximately every 36 days the spacecraft must perform a yaw maneuver.

[5] Constituent data are provided on a grid with 6 levels per factor of 10 in pressure, i.e., 100, 68.1, 46.4, 31.6, 21.5, 14.7, 10 hPa, and so on. The vertical spacing of these grid levels is approximately 2.7 km. CLAES and MLS have similar viewing geometry and frequency of profiles, and for both data sets we use L3AT data (in which data are interpolated to a standard set of profiles along the viewing track) from the most recent version.

[6] For this study we focus on the tropics, i.e., latitudes between  $27.5^{\circ}\text{S}$  and  $27.5^{\circ}\text{N}$ . The profile data are first averaged using bins of width  $24^{\circ}$  longitude and  $5^{\circ}$  latitude for each day. While the longitudinal resolution may seem very coarse, it is ample for resolving the features of interest, which tend to have most of their power in zonal wavenumbers 1 and 2. On most days there are over 500 profiles within this latitude band (out of a global total of over 1300 per day), and consequently the typical bin contains about three profiles. Since we are focusing on timescales longer than  $\sim 4$  days and on a phenomenon with essentially no diurnal dependence, the results should be insensitive to the fact that we have ignored the local time of observation.

[7] The time period studied here stretches from July 1992 to late April 1993, the period of record with the densest,

highest-quality trace constituent measurements. All data are band-pass-filtered (4–90 days), to remove the seasonal cycle and variations at high frequencies that might be affected by aliasing with the satellite’s orbit.

## 2.1. Microwave Limb Sounder

[8] The Microwave Limb Sounder (MLS) [Barath *et al.*, 1993] retrieves temperature and constituent data from microwave emissions using three radiometers (at 63, 183, and 205 GHz). Version 5 (V5) data are used for temperature and ozone [Livesey *et al.*, 2003]. Small temporal gaps (all but two of which are only one day long) are filled by linear interpolation in time for analyses, but not in Figure 2 where the gaps are visible.

### 2.1.1. MLS Temperature

[9] The MLS V5 algorithm retrieves temperatures above the 68 hPa pressure level on every UARS surface, but the range of most reliable temperatures is 32–0.46 hPa; MLS still contributes some information at 46 hPa, but very little at 68 hPa. The Kelvin wave signature in this data set was described by Mote *et al.* [2002]; they found coherent Kelvin wave variations down to 68 hPa, despite the poor data quality there. The mean tropical profile of MLS temperature is shown in Figure 1a.

### 2.1.2. MLS Ozone

[10] Two separate MLS ozone products [Froidevaux *et al.*, 1996] are retrieved, one using the 205 GHz radiometer and one using the 183 GHz radiometer. The 183-GHz radiometer failed in late April 1993. Here we use only data from the 205 GHz radiometer, as these data are more accurate in the stratosphere [Froidevaux *et al.*, 1996]. Accuracy is very good (order of 5%) in most of the stratosphere, but errors increase sharply approaching the tropical tropopause (exceeding 50% at 100 hPa) owing to the very low ozone values there. We use data from 46 to 0.68 hPa (Figure 1c).

## 2.2. CLAES

[11] The Cryogenic Limb Array Etalon Spectrometer (CLAES) retrieves temperature and constituent data from infrared emissions [Roche *et al.*, 1993]. An array of stacked detectors, each pointing at a different 2.5-km-thick vertical slice of the limb, provided simultaneous vertical coverage from 10 to 60 km. To prevent the instrument’s own thermal emissions from interfering with the atmospheric signal, the instrument was cooled with cryogenics; the cryogenics finally evaporated on May 5, 1993, ending the CLAES period of observations. Nine blocking filters each pass a certain narrow frequency band of incoming infrared radiation. Temperature is retrieved using filter 8 (centered on  $792\text{ cm}^{-1}$ ) [Gille *et al.*, 1996], ozone using filter 8 and filter 9 ( $780\text{ cm}^{-1}$ ) [Bailey *et al.*, 1996], CFC-12 ( $\text{CF}_2\text{Cl}_2$ ) using filter 5 ( $923\text{ cm}^{-1}$ ) [Nightingale *et al.*, 1996], and methane ( $\text{CH}_4$ ) and nitrous oxide ( $\text{N}_2\text{O}$ ) using filter 4 ( $1257\text{ cm}^{-1}$ ) [Roche *et al.*, 1996]. Although we analyzed CFC-12 and methane data, the results were ambiguous and we do not present them here. The validation papers cited here referred to CLAES V7; in this paper we use CLAES V9, and note below any significant changes from the V7 data.

[12] Around the time of each UARS yaw maneuver, the CLAES instrument’s aperture door was closed for several days to protect the instrument from sunlight [Bailey *et al.*, 1996]. These data gaps are sufficiently frequent, lengthy,

and periodic that we do not attempt to fill the gaps by interpolation as we do with MLS.

### 2.2.1. CLAES Temperature

[13] Correlative measurements for temperature are far more numerous than for trace constituents, and include radiosondes, ground-based lidar, and the reanalyses of the National Centers for Environmental Prediction (NCEP) and the United Kingdom Meteorological Office (UKMO). *Gille et al.* [1996] note a global cold bias of about 2K in V7; the bias in V9 is near zero. They also note differences with NCEP and UKMO in latitude-pressure sections, which they attribute to tropical waves of the sort examined in this paper; such waves would elude the nadir-viewing TOVS instrument that forms the basis for the reanalysis data. Indeed, as M02 noted, NCEP and UKMO data do not exhibit the Kelvin wave variations seen in MLS.

[14] The CLAES temperature retrieval extends down to the 316 hPa level, and errors with respect to radiosondes are small (1–2 K) at 146 and 215 hPa. CLAES provides estimates of temperature well below the lowest valid MLS level, though we presume the measurements will be obscured by clouds and hence biased toward cloud-free conditions. At the levels where both CLAES and MLS report temperature values, CLAES is consistently higher (Figure 1a) and has more variance (Figure 1b).

### 2.2.2. CLAES Ozone

[15] CLAES ozone measurements agree well with correlative measurements throughout the altitude range of the stratosphere [*Bailey et al.*, 1996], though most of these correlative measurements were taken in middle or high latitudes. In the tropics below the peak in the ozone profile, possible contamination by volcanic aerosol is a concern, but the good agreement with MLS ozone (Figure 1c) is reassuring, because MLS measurements are unaffected by aerosol. The differences between MLS and CLAES in the mean profiles are consistent with the slight high bias of CLAES ozone near 10 hPa and low bias in the upper stratosphere [*Bailey et al.*, 1996]. Tropical ozone values below 20 hPa are several tenths of a ppmv lower in V9 than in V7, with large percentage reductions (greater than 50%) just above the tropopause; these reductions bring it into line with MLS observations.

### 2.2.3. CLAES Nitrous Oxide (N<sub>2</sub>O)

[16] Methane and nitrous oxide are both retrieved by the same filter (4) on CLAES. The vertical profile of CLAES nitrous oxide (Figure 1e) is similar to methane (not shown), including an unexplained local maximum in the lower stratosphere. This feature is a departure from the expected profile (monotonic decrease with altitude), since these constituents have near-monotonic increases with time in the troposphere, no sources in the stratosphere and a photochemical sink in the upper stratosphere. Although a disturbance in stratospheric circulation by the Mt. Pinatubo eruption is a possible explanation, the modeling work of *Considine et al.* [2001] suggests that the changes in circulation would be insufficient to generate a local maximum as observed in CLAES data. The facts that (1) other constituents observed by CLAES (methane, CFC-12) show a similar feature, (2) methane data from the Halogen Occultation Experiment show no such feature in 1992 and 1993, and (3) the feature was stronger in V7 data, all suggest that it may be a retrieval

problem associated with the vestiges of the Pinatubo aerosol cloud.

[17] Nitrous oxide observations have limited correlative measurements in the tropics, but globally, the CLAES V7 N<sub>2</sub>O data are biased slightly low (by less than 15%) below 7 hPa. The V9 data are substantially lower than V7 in the tropical lower stratosphere and have a more accentuated local maximum, though globally the differences between V9 and correlative data are smaller.

## 3. Description of Variations in Temperature and Trace Constituents

[18] Variations associated with Kelvin waves represents a substantial fraction (20–40%) of total variance at subseasonal timescales (dashed lines in Figures 1b, 1d and 1f). We describe these variations in several ways.

[19] As in M02, the three-dimensional stratospheric variations in the fields of interest (temperature, ozone, and nitrous oxide) are initially reduced to one dimension by taking the projection of the field onto the cosine of longitude, along the equator (Figure 2). The same projection is done for the sine of longitude; these are not shown, but are substantially similar to those for the cosine.

[20] Downward propagating features are clearly evident in MLS temperature (Figure 2a) and were discussed by M02. Of particular interest are the large-amplitude events in September 1992 and January–February 1993. M02 identified two distinct modes in the  $k = 1$  MLS temperature variations shown in Figure 2a, and verified that both satisfied the dispersion relation for Kelvin waves. The one that is most obvious in Figure 2a has period near 10 days, vertical wavelength 20 km in the upper stratosphere, and horizontal phase speed  $48 \text{ ms}^{-1}$ . The less obvious mode has a period of 6.5 days, vertical wavelength 23 km, and horizontal phase speed  $71 \text{ ms}^{-1}$ . It has largest amplitude in December 1992 and January 1993.

[21] There is a very good correspondence between the variations in MLS temperature and those in CLAES temperature (Figure 2b). CLAES has the advantage of extending into the troposphere, and it appears that the variations noted in the MLS data are linked to variations at 100 hPa. As will be seen below, these coherent variations continue into the upper troposphere.

[22] MLS ozone data (Figure 2c) also clearly show downward propagating features, and most correspond well to the temperature variations. However, in the lower stratosphere, the predominant variations have longer period and smaller vertical phase speed. These features are especially prominent in August–September 1992 and also appear in late January 1993. It is difficult to identify by eye the expected phase reversal that should accompany the change in sign of the vertical gradient at around 10 hPa (Figure 1c).

[23] Unfortunately, CLAES ozone data Figure 2d are too noisy to reveal clearly the same sorts of variations that are shown in Figure 2c. There are intriguing suggestions of the same descending features, especially in August–September 1992, as those in MLS. The variance is larger than with MLS ozone data (Figure 1d).

[24] The story is similar with other CLAES constituents including nitrous oxide (Figure 2e): Downward propagating features appear at various times. Statistical analysis of

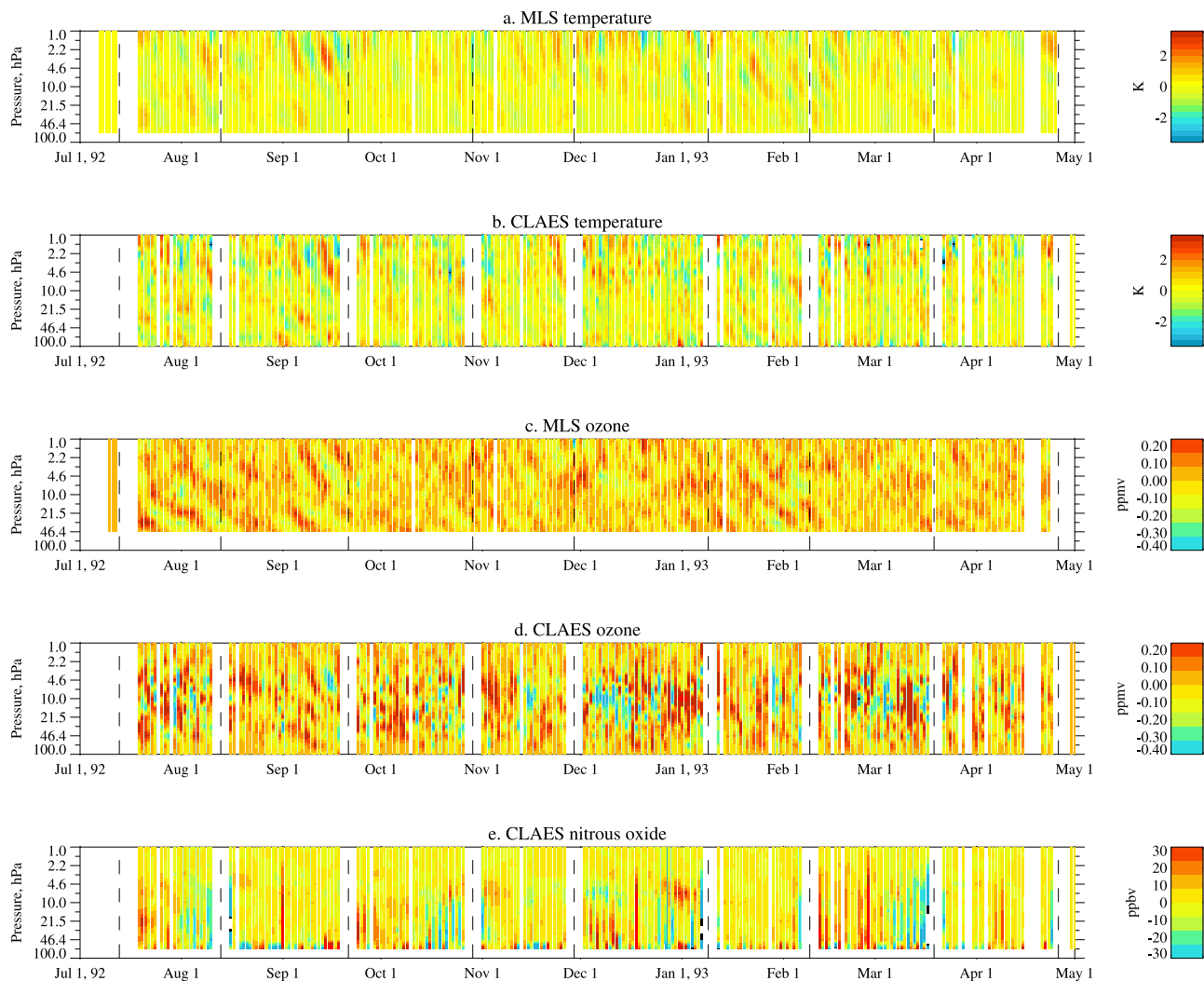


**Figure 2.** Time-height plots of the wavenumber-one component (cosine) along the equator of the field indicated. Contour interval for temperature (a, b) is 0.4K; for ozone (c, d), 0.1 ppmv; and for nitrous oxide (e), 8 ppbv. Vertical dashed lines denote days when the UARS performed a yaw maneuver; the CLAES instrument was shut off for several days around each yaw day. The mean during each yaw cycle was removed in order to account for a small yaw-dependent bias, which mainly affected CLAES ozone.

these data reveal more connections than are evident in Figure 2.

### 3.1. Spectral Analysis

[25] Gaps in CLAES data (Figure 2) are too numerous for spectral analysis to work well, but MLS data are nearly continuous. We perform spectral analysis by wavenumber and frequency at each of the latitudes and altitudes in the study domain, as in M02, but now for both temperature and ozone from MLS. For temperature (Figure 3), there is a sharp spectral peak at about 10 days, part of a band of spectral power between roughly 7.5 and 11.5 days. Note that the extended empirical orthogonal function (EEOF) analysis of the same data by M02 led to a spectral peak at about 9.6 days. There are other peaks in the intraseasonal range and near 6 days, corresponding to the second mode identified by M02.

[26] Spectral power is strongly concentrated in wavenumber 1 (Figure 3b), especially for eastward (positive)

wavenumber 1. The meridional distribution (Figure 3c) shows a peak at the equator, diminishing toward the subtropics. Beyond  $15^\circ$  (not shown), power rises again owing to midlatitude waves.

[27] The vertical profile of spectral power (Figure 3d) shows a near-monotonic increase with height, despite the decrease in overall variance from 100 hPa to 22 hPa (Figure 1b). The overall variance includes seasonal and zonal variations, which are excluded from the analysis here; seasonal variations in temperature are strongest near the tropopause and diminish sharply with altitude [Reed and Vlcek, 1969], accounting for the differences between Figures 1b and 3d. At every level the spectral power in the 5–30 day band accounts for nearly all of the power in the frequency band analyzed here (roughly 4–90 days).

[28] For ozone, the largest spectral peak (Figure 4a) is near 10 days, as for temperature, but the rest of the spectrum is somewhat redder (more variance at low frequencies) for ozone than for temperature. The wavenumber dependence

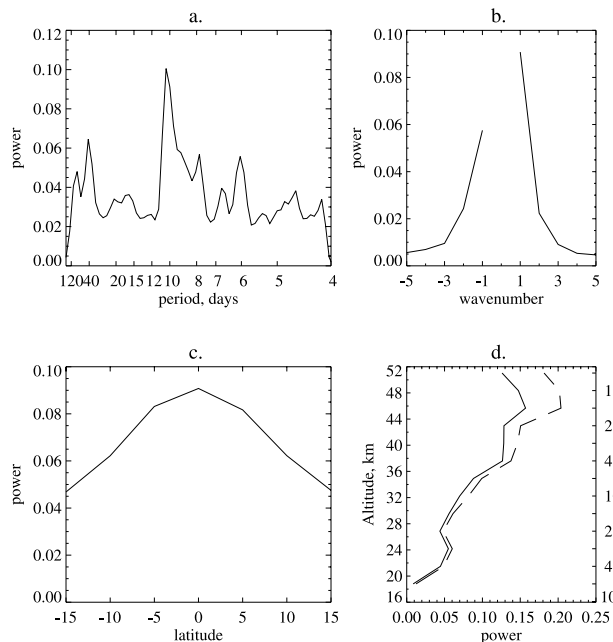


**Figure 3.** Spectral power ( $K^2$ ) of variations in temperature from the MLS instrument, viewed as functions of (a) period, (b) zonal wavenumber, (c) latitude, and (d) altitude. In panel (a), power along the equator has been summed over altitude and over positive zonal wavenumbers, then smoothed once with a 1-2-1 filter. Power drops to zero near the limits of the band-pass filtering (4–90 days). In panel (b), power along the equator in the 5–30 day frequency band has been summed in altitude. In panel (c), power for zonal wavenumber 1 ( $k = 1$ ) has been summed in altitude and over the 5–30 day frequency band. Panel (d) shows spectral power at the equator for  $k = 1$  summed over the 5–30 day frequency band (solid) and over the 4–90 day band (dashed).

(Figure 4b) is similar to that for temperature, with eastward  $k = 1$  dominant followed by westward  $k = 1$  and substantially less power at higher wavenumbers. The latitude dependence of  $k = 1$  spectral power (Figure 4c) is also similar to that for temperature, peaked at the equator and falling to about half that value at  $15^\circ$  latitude.

[29] Only the vertical dependence (Figure 4d) of spectral power is substantially different from that of temperature; maxima in the lower and upper stratosphere are separated by a minimum at the altitude of the ozone maximum, as expected (since perturbations depend on  $\partial O_3/\partial z$ , and  $\partial O_3/\partial z \simeq 0$  near 10 hPa). *Randel* [1990] obtained a similar result using LIMS V5 data, but the results were quite different in LIMS V4 data (his Figure 3). There are two reasons the spectral peak for ozone in the lower stratosphere should be larger than the one in the upper stratosphere even though the spectral peak for temperature in the upper stratosphere is larger: First, the vertical gradient is relatively larger in the lower stratosphere (this can be seen by plotting  $dO_3/dT$  versus altitude) and second, the photochemical timescale for ozone is short in the upper stratosphere, so it adjusts rapidly to perturbations in temperature [*Randel*, 1990].

[30] Having examined the variations in temperature and ozone separately, we now examine their co-variation. The

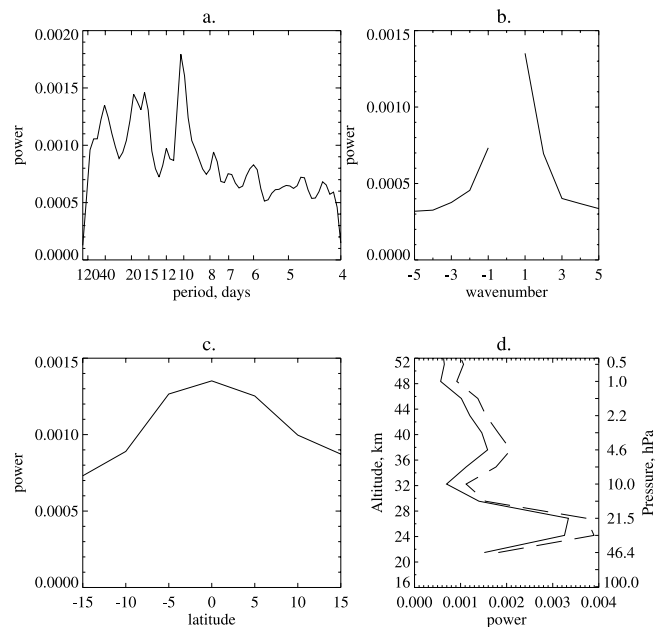


**Figure 4.** As in Figure 3 but for MLS ozone ( $\text{ppm}^2$ ).

cross-spectrum  $\Gamma_{xy}(\omega)$  at frequency  $\omega$  can be calculated as the Fourier transform of the cross-covariance function  $\gamma_{xy}$ :

$$\Gamma_{xy}(\omega) = \sum_{\tau=-\infty}^{\infty} \gamma_{xy}(\tau) e^{-2\pi i \tau \omega}$$

[*von Storch and Zwiers*, 2001]. These are calculated for both sine and cosine components of  $k = 1$  at each level, then averaged. (This approach does not distinguish between eastward traveling and westward traveling waves; however, the spectral power in eastward traveling waves at  $k = 1$  is roughly twice the power for westward traveling waves (see Figures 3 and 4).) Figure 5 shows how the amplitude of the cross spectrum for temperature and ozone depends on altitude and period. Since both fields have a spectral peak near 10 days, it is no surprise that the largest peak in the coherence squared is also near 10 days. It gives the appearance of tending toward shorter periods as altitude increases, and there is a minimum at 10–20 hPa as

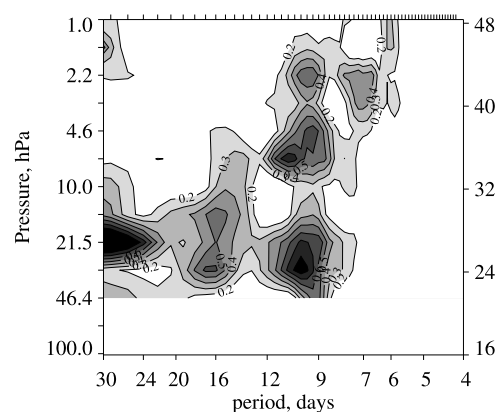


**Figure 5.** Squared coherence of temperature and ozone as a function of altitude and period.

expected. There is also a broad, shallow peak in the lower stratosphere at about 17 days (see Figure 4; the feature appears as the second pair of EEOFs of ozone, not shown) and a sharp peak at about 7 days (see Figure 3) in the upper stratosphere.

### 3.2. Regression

[31] M02 calculated extended empirical orthogonal functions (EEOFs) of MLS temperature data and used the first principal component (PC) to find the three-dimensional structure of the 10-day Kelvin mode by regression. Regression analysis is more suitable for the gappy CLAES data than analysis requiring continuous time series, e.g., spectral analysis or EEOF analysis. We use the same reference time series, i.e., the first PC of MLS temperature data, and regress MLS and CLAES temperature, MLS and CLAES ozone, and CLAES  $\text{N}_2\text{O}$ ,  $\text{CH}_4$ , and  $\text{CF}_2\text{Cl}_2$  (all but the last two of these are shown in Figure 6). Analysis has been performed separately at each latitude and the results are averaged between  $5^\circ\text{S}$  and  $5^\circ\text{N}$ . To test significance, a Monte Carlo approach is used in which for each field at each altitude, we generate 1000 random time series with variance matched to the observed field at that altitude (Figure 1). Regression analysis is performed and results averaged in latitude as with observations. Locations where the regression coefficient is statistically significant ( $\alpha = 0.1$ ) are hatched (/ for the reference time series from EEOF1, \ for the time series from EEOF2). Regression coefficients for temperature and ozone are significant almost everywhere; for  $\text{N}_2\text{O}$  only in a few places, but in physically reasonable patterns. For methane and CFC-12 (not shown), regression coefficients do not match up with the phase lines and significance is no greater than would be expected by chance.

[32] The amplitude of the CLAES variations in temperature and ozone (Figures 6b and 6d) is slightly greater than for the MLS variations, especially for negative temperature anomalies which are about twice as big as those in MLS. A partial explanation for the higher amplitude is the larger overall variance of CLAES temperatures (Figure 1b); though the ratio of variances is smaller than the ratio of 10-day Kelvin wave amplitudes, it is possible that for the 10-day band the ratio of variances is larger than for other bands (compare Figures 2a and 2b). A more perplexing difference between MLS and CLAES occurs in the lowermost stratosphere, where the phase lines no longer coincide between the two data sets. A possible explanation is that the leading EEOF in MLS temperature has largest variance in the upper stratosphere, and when performing regression, other variance can creep in; the lower stratospheric variations in CLAES may not be as coherent with the upper stratospheric variations as is the case in MLS. A more likely explanation lies in the differing vertical resolutions of the two instruments: CLAES precision is best at 100 hPa [Gille *et al.*, 1996] but MLS loses temperature sensitivity in the lower stratosphere and the retrieved profile is smoothed, hence decreasing the resolvable vertical scale (D. Wu, personal communication, 2002). The fact that the CLAES anomalies extend to 100 hPa is an intriguing possible connection to stratosphere-troposphere exchange.

[33] MLS ozone (Figure 6c) offers only hints of a relationship to temperature, though these will become

clearer shortly. The phase lines seem to have roughly the same slope as for temperature, and there are hints of a sign change at the ozone maximum (10 hPa).

[34] All of these features are clearer in CLAES ozone (Figure 6d), revealed by the regression analysis despite the difficulty of identifying them visually in Figure 2. The most prominent feature starts at  $0^\circ$  longitude, 21.5 hPa, as a negative anomaly approximately in phase with temperature; just above 10 hPa, it changes sign and is roughly out of phase with temperature. Along other phase lines, one can see similar features, though not as consistently. The CLAES ozone data provide a guide for identifying consistent features in MLS ozone. As with temperature, the variations in ozone are larger in CLAES data than MLS data, owing perhaps in part to larger overall variance (Figure 1d).

[35] Perturbations in CLAES nitrous oxide (Figure 6e) line up well with the phase lines and are of the expected sign, i.e., opposite to that of temperature. The pattern breaks down in the lowest part of the stratosphere where the vertical gradient changes sign. In the upper stratosphere, the variations become very small as the background values of nitrous oxide approach zero (Figure 1e).

[36] As a means to examine the possible influence of constituent retrievals on the regression results, we use a simple 1-d transport model (neglecting photochemistry, which is important for ozone in the upper stratosphere) to construct artificial Kelvin wave variations from the first two EEOFs of temperature using the assumption that Kelvin waves affect a trace constituent  $\mu$  primarily by displacing isopleths of  $\mu$  (or  $T$ ) up or down:

$$\mu'_{Ti} = T'_i \bar{\mu}_z \quad (1)$$

where  $\bar{\mu}_z$  is the vertical gradient of  $\mu$ ,  $T'_i$  is the temperature perturbation associated with the  $i$ th EEOF, and  $\bar{T}_z$  is the vertical gradient of time mean, zonal mean temperature.

[37] Using these  $\mu'$  time series for each trace constituent (plus temperature), we again perform regressions using as reference time series the first two EEOFs of MLS temperature. Figure 7 compares the root-sum-square of the regression coefficients for the first two EEOFs (dashed lines) with the equivalent for the real data (solid lines). For temperature, the results are rather similar. For ozone, the observed CLAES data have a double peak in the regression coefficients at roughly 2 and 20 hPa, as with the simulated ozone data. (The correspondence between ozone and temperature in the upper stratosphere is in fact dominated by photochemistry, not transport, but the effect is of the same sign.) MLS ozone also has the double peak but the regression coefficients are much smaller. Nitrous oxide regression results do not agree well with the values predicted by the 1-d model except in the upper part of the domain. These results suggest that the instruments are more successful at detecting Kelvin wave-induced fluctuations in temperature and ozone than in the other trace constituents, for which the perturbations should be considerably larger than observed.

## 4. Conclusions

[38] UARS data offer another look at the influence of Kelvin waves on stratospheric trace constituents. The

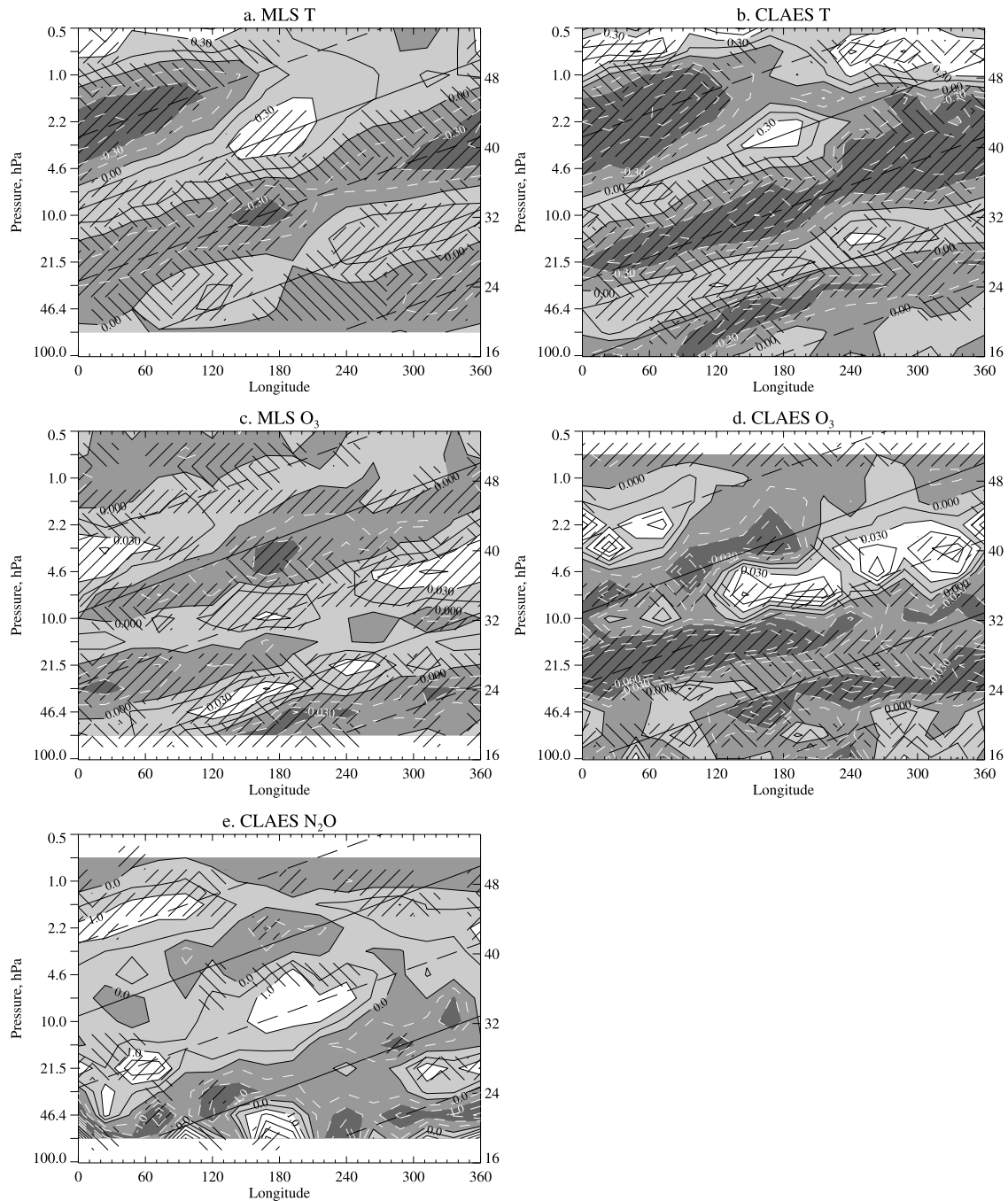


**Figure 6.** The field indicated in each panel's title has been regressed on a reference time series, the first principal component of extended EOF of MLS temperature (see text for details). Approximate phase lines are indicated in each panel; they have been derived from panel *a* by calculating best-fit lines to the profile maximum and minimum at each longitude. Panel *a* shows MLS temperature data; *b*: As in *a* but for CLAES temperature data. Contour interval in panels *a* and *b* is 0.15 K. Panels *c* and *d* show ozone data from MLS and CLAES, respectively; contour interval 0.015 ppmv. Panel *e* shows CLAES nitrous oxide, contour interval 0.5 ppbv. Values plotted are derived from a dimensionless reference time series, but a fluctuation of 1 K in panel *a* corresponds roughly to 0.15 ppmv in ozone and 7 ppbv in nitrous oxide.

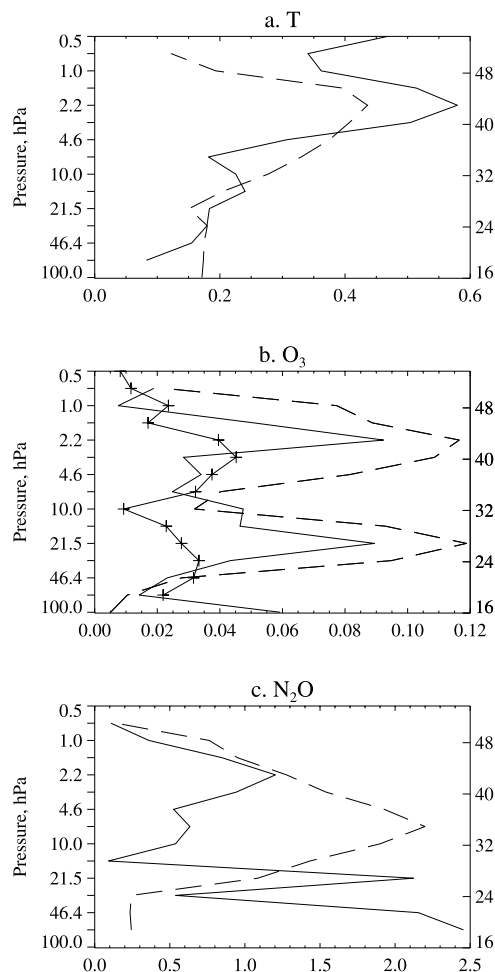


**Figure 7.** Comparison of regression coefficients on the equator for real data (solid curves) and data generated by a 1-D model (equation (1)) using the first two EEOFs of MLS temperature. See text for details.

roughly 10-day Kelvin wave mode identified by M02 appears also in the ozone and nitrous oxide data, as revealed variously in Figure 2 (especially September 1992 and January–February 1993) and by the coherence and regression calculations in Figures 5 and 6 (and also EEOFs, not shown).

[39] Kelvin waves are the dominant mode of tropical intraseasonal (4–90 days) variability in the stratosphere, for both temperature and ozone (Figures 3 and 4), with sharp spectral peaks at around 10 days for  $k = 1$ , and with a maximum variance at the equator. Other trace constituents, like  $\text{CH}_4$ ,  $\text{N}_2\text{O}$ , and  $\text{CF}_2\text{Cl}_2$ , probably have similar spectral characteristics, but these constituents are measured only by CLAES and spectral analysis does not work well for CLAES data owing to the long and frequent gaps.

[40] Important differences appear when the same field is examined from two different satellite data sets. CLAES data (both temperature and ozone) showed generally larger responses to the same Kelvin wave than did MLS data. Though the phases appeared to be similar for the two data sets for ozone, for temperature there were significant differences in the lower stratosphere, possibly owing to different vertical resolution there, with CLAES more likely to be

correct. The regression coefficients derived from CLAES ozone more closely resembled those expected from our simple 1-d model (Figure 7).

[41] Ground-based observations of stratospheric Kelvin waves can resolve much finer vertical scales, and such observations paint a somewhat different picture of Kelvin wave behavior with higher vertical and zonal wavenumbers [e.g., Holton *et al.*, 2001]. This implies that the dominant Kelvin mode in any data set depends on the observing characteristics of the instrument, a point made by Alexander [1998] for gravity waves. Although MLS and CLAES have similar viewing geometries (cool-side, limb-viewing) and vertical resolution, they end up with subtle but important differences in the structure of retrieved Kelvin waves (Figure 6). Future satellite missions with high vertical resolution, notably EOS-MLS and HIRDLS, may yield different leading modes; in any case, they will afford a more comprehensive look at variations in temperature and important trace constituents.

[42] **Acknowledgments.** Aiden Roche provided helpful comments on an earlier draft of this manuscript, especially with regards to CLAES data. We thank Dong Wu for helpful discussions, and gratefully acknowledge the accomplishments of the MLS and CLAES instrument teams. This work was supported by NASA contracts NAS1-99130, NAS5-98078, and NAS5-01154.

## References

- Alexander, M. J. (1998), Interpretations of observed climatological patterns in stratospheric gravity wave variance, *J. Geophys. Res.*, *103*, 8627–8640.
- Bailey, P. L., et al. (1996), Comparison of cryogenic limb array etalon spectrometer (CLAES) ozone observations with correlative measurements, *J. Geophys. Res.*, *101*, 9737–9756.
- Barath, F. T., et al. (1993), The Upper Atmosphere Research Satellite Microwave Limb Sounder instrument, *J. Geophys. Res.*, *98*, 10,751–10,762.
- Canziani, P. O., and J. R. Holton (1998), Kelvin waves and the quasi-biennial oscillation: An observational analysis, *J. Geophys. Res.*, *103*, 31,509–31,521.
- Canziani, P. O., J. R. Holton, E. F. Fishbein, L. Froidevaux, and J. W. Waters (1994), Equatorial Kelvin waves: A UARS MLS view, *J. Atmos. Sci.*, *51*, 3053–3076.
- Canziani, P. O., J. R. Holton, E. F. Fishbein, and L. Froidevaux (1995), Equatorial Kelvin wave variability during 1992 and 1993, *J. Geophys. Res.*, *100*, 5193–5202.
- Considine, D. B., J. E. Rosenfield, and E. L. Fleming (2001), An interactive model study of the influence of the Mount Pinatubo aerosol on stratospheric methane and water trends, *J. Geophys. Res.*, *106*, 27,711–27,727.
- Froidevaux, L., et al. (1996), Validation of UARS Microwave Limb Sounder ozone measurements, *J. Geophys. Res.*, *101*, 10,017–10,060.
- Fujiwara, M., K. Kita, and T. Ogawa (1998), Stratosphere-troposphere exchange of ozone associated with the equatorial Kelvin wave as observed with ozonesondes and radiosondes, *J. Geophys. Res.*, *103*, 19,173–19,182.
- Fujiwara, M., F. Hasebe, M. Shiotani, N. Nishi, H. Vömel, and S. J. Oltmans (2001), Water vapor control at the tropopause by the equatorial Kelvin wave observed over Galápagos, *Geophys. Res. Lett.*, *28*, doi:10.1029/2001GL013310.
- Gille, J. C., et al. (1996), Accuracy and precision of the Cryogenic Limb Array Spectrometer (CLAES) temperature retrievals, *J. Geophys. Res.*, *101*, 9583–9601.
- Holton, J. R., M. J. Alexander, and M. T. Boehm (2001), Evidence for short vertical wavelength Kelvin waves in the Department of Energy–Atmospheric Radiation Measurement Nauru99 radiosonde data, *J. Geophys. Res.*, *106*, 20,125–20,129.
- Kawamoto, N., M. Shiotani, and J. C. Gille (1997), Equatorial Kelvin waves and corresponding tracer oscillations in the lower stratosphere as seen in LIMS data, *J. Meteorol. Soc. Jpn.*, *75*, 763–773.
- Livesey, N. J., W. G. Read, L. Froidevaux, J. W. Waters, M. L. Santee, H. C. Pumphrey, D. L. Wu, Z. Shippony, and R. F. Jarnot (2003), The UARS Microwave Limb Sounder version 5 data set: Theory, characterization and validation, *J. Geophys. Res.*, *108*, doi:10.1029/2002JD002273.



- Mote, P. W., T. J. Dunkerton, and D. Wu (2002), Kelvin waves in stratospheric temperature observed by the Microwave Limb Sounder, *J. Geophys. Res.*, *107*, doi:10.1029/2001JD001056.
- Nightingale, R. W., et al. (1996), Global CF<sub>2</sub>Cl<sub>2</sub> measurements by UARS cryogenic limb array etalon spectrometer: Validation by correlative data and a model, *J. Geophys. Res.*, *101*, 9711–9736.
- Randel, W. J. (1990), Kelvin wave-induced trace constituent oscillations in the equatorial stratosphere, *J. Geophys. Res.*, *95*, 18,641–18,652.
- Reber, C. A., C. E. Trevathan, R. J. McNeal, and M. R. Luther (1993), The Upper Atmosphere Research Satellite (UARS) Mission, *J. Geophys. Res.*, *98*, 10,643–10,647.
- Reed, R. J., and C. L. Vlcek (1969), The annual temperature variation in the lower tropical stratosphere, *J. Atmos. Sci.*, *26*, 163–167.
- Roche, A. E., J. B. Kumer, J. L. Mergenthaler, G. A. Ely, W. G. Uplinger, J. F. Potter, T. C. James, and L. W. Sterritt (1993), The Cryogenic Limb Array Etalon Spectrometer (CLAES) on UARS: Experiment description and performance, *J. Geophys. Res.*, *98*, 10,763–10,775.
- Roche, A. E., et al. (1996), Validation of CH<sub>4</sub> and N<sub>2</sub>O measurements by the CLAES instrument on the Upper Atmosphere Research Satellite, *J. Geophys. Res.*, *101*, 9679–9710.
- Shiotani, M., J. C. Gille, and A. E. Roche (1997), Kelvin waves in the equatorial lower stratosphere as revealed by cryogenic limb array etalon spectrometer temperature data, *J. Geophys. Res.*, *102*, 26,131–26,140.
- Smith, A. K., P. Preusse, and J. Oberheide (2002), Middle atmosphere Kelvin waves observed in Cryogenic Infrared Spectrometers and Telescopes for the Atmosphere (CRISTA) 1 and 2 temperature and trace species, *J. Geophys. Res.*, *107*, doi:10.1029/2001JD000577.
- von Storch, H., and F. W. Zwiers (2001), *Statistical Analysis in Climate Research*, Cambridge Univ. Press, New York.
- Wallace, J. M., and V. E. Kousky (1968), Observational evidence of Kelvin waves in the tropical stratosphere, *J. Atmos. Sci.*, *25*, 900–907.

---

T. J. Dunkerton and P. W. Mote, Northwest Research Associates, P.O. Box 3027, Bellevue, WA 98009, USA. (tim@nwra.com; mote@nwra.com)